

© 2021 IEEE. Personal use of this material is permitted. Permission from IEEE must be obtained for all other uses, in any current or future media, including reprinting/republishing this material for advertising or promotional purposes, creating new collective works, for resale or redistribution to servers or lists, or reuse of any copyrighted component of this work in other works.

A. P. Jovanović, M. N. Stankov, D. Loffhagen, and M. M. Becker, "Automated Fluid Model Generation and Numerical Analysis of Dielectric Barrier Discharges Using Comsol," *IEEE Trans. Plasma Sci.*, vol. 49, pp. 3710-3718, 2021, doi: 10.1109/TPS.2021.3120507.

URL: <https://ieeexplore.ieee.org/document/9600812>

# Automated fluid model generation and numerical analysis of dielectric barrier discharges using Comsol

Aleksandar P. Jovanović , Marjan N. Stankov , Detlef Loffhagen , Markus M. Becker 

**Abstract**—MCPlas is introduced as a powerful tool for automated fluid model generation with application to the analysis of dielectric barrier discharges operating in different regimes. MCPlas consists of a number of MATLAB® scripts and uses the COMSOL Multiphysics® module LiveLink™ for MATLAB® to build up equation-based COMSOL Multiphysics® models from scratch. The present contribution highlights how MCPlas is used to implement time-dependent models for non-thermal plasmas in spatially one-dimensional and axisymmetric two-dimensional geometries and stresses out the benefit of automation of the modelling procedure. The modelling codes generated by MCPlas are used to study diffuse and filamentary dielectric barrier discharges in argon at sub-atmospheric and atmospheric pressure, respectively. The seamless transition between different levels of model complexity with respect to the considered model geometry is demonstrated. The presented investigation of a single-filament dielectric barrier discharge interacting with a dielectric surface shows that complex phenomena of high technological relevance can be tackled by using plasma models implemented in COMSOL Multiphysics® via MCPlas.

**Index Terms**—Plasma modelling, Automation, Discharges (electric).

## I. INTRODUCTION

**D**IELECTRIC barrier discharges (DBDs) are frequently used to generate non-thermal plasmas for technological applications, such as ozone generation, surface processing and plasma medicine [1]–[5]. DBDs are characterised by the presence of a dielectric layer on at least one electrode, which limits the electric current and prevents transition to an arc plasma. Depending on the conditions, DBDs can be diffuse or filamentary, in some cases self-organised patterns occur [6]. Due to their broad use, it is of crucial importance to get a detailed understanding of the physical and chemical processes occurring in DBDs. A common way to do this is by applying fluid-Poisson models, which couple fluid equations for the plasma species with Poisson’s equation for the electric potential [7]–[13]. The computational efficiency of these models allows one to take into account complex physical and chemical processes occurring during the plasma production, which makes them suitable for practical applications.

In the present manuscript, a toolbox combining functionalities of COMSOL Multiphysics® [14] (in further text Comsol) and MATLAB® [15] (in further text Matlab), named MCPlas, is introduced for the automated implementation of fluid-Poisson models in Comsol. MCPlas consists of a number

of Matlab scripts using the functionality provided by the COMSOL module LiveLink™ for MATLAB® (in further text Livelink module) to build up the plasma models in Comsol. This replaces the manual definition of equations, which becomes a tedious and error-prone process for complex models often taking into account tens to hundreds of species and hundreds to thousands of reaction kinetic processes [16]–[20]. Therefore, the main aim of this work is to stress out the benefit of automation and to illustrate how this can be achieved by using MCPlas.

In order to illustrate the use of MCPlas for automated code implementation, two test cases are presented: 1) a diffuse DBD in argon at sub-atmospheric pressure, and 2) a filamentary atmospheric-pressure DBD in argon. The numerical results obtained for these application cases are analysed in detail to explain the main features of the different discharges. The present study substantially extends the initial results presented in [21] and demonstrates the wide-range applicability of MCPlas. An earlier, simplified version of MCPlas was applied in the benchmark simulation study on positive streamers in air [22].

The paper is structured as follows. Section II introduces the MCPlas toolbox by illustrating the structure of the code and describing its main features. The results and discussion section III describes the fluid-Poisson model implementation obtained from MCPlas and introduces the two case studies as exemplary applications. Finally, main conclusions are given in section IV.

## II. MCPLAS TOOLBOX

The Matlab-Comsol toolbox for plasma modelling was developed for automated implementation of fluid-Poisson models in Comsol. It consists of a number of Matlab scripts and uses the Livelink module to set up the system of partial differential equations using equation-based modelling. This means that all equations are implemented on the basis of the basic differential equation interfaces in Comsol without using additional modules.

The workflow for the implementation and usage of a plasma model in Comsol using MCPlas is visualised in Fig. 1. The first step in the Matlab code sets up the relevant parameters. This includes information about the discharge geometry, specific domains (plasma, dielectric etc.), boundary selections (e.g. powered electrode, grounded electrode, dielectric-plasma interface), and modelling procedure. Depending on these parameters, the geometry is defined and a proper form of coordinates

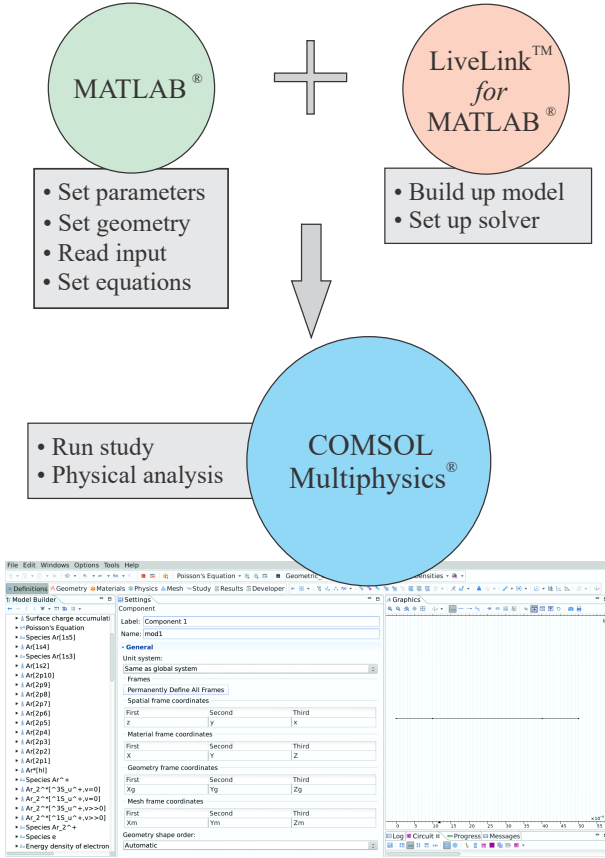


Fig. 1. Model generation and analysis workflow of MCPlas.

(Cartesian or cylindrical), boundary system, and the equations are implemented.

The input data consists of a list of the plasma species considered, their properties, and plasma-chemical reactions together with rate and transport coefficients. This input data is read in next. It is important to note that the implementation of all balance equations with corresponding reaction kinetic processes is automated by using the species list and reaction kinetic scheme prepared in advance. These input files specify which species, collision processes and radiation processes are taken into account, and directly determine the balance equations to be solved. The input data also specify the set of physically motivated boundary conditions and initial values to complete the coupled system of partial differential equations.

After these steps, the Livelink module is employed to build up a Comsol model by setting up the definitions of physical quantities, coefficients and governing equations with their initial and boundary conditions. Additional input variables are used to set up the numerical solver for efficient solution of the nonlinear coupled system of equations. Note that MCPlas is able to automatically generate plasma models in Comsol involving an arbitrary number of species and reaction kinetic processes depending on the general input files defined by the user. While the general set of equations and boundary conditions are pre-defined by the MCPlas code, the gas (mixture), number of considered species, reaction kinetic scheme, geometry, and external discharge parameters can be changed

by the user via the input parameters and input files.

The last step in the modelling process is to run the study, which can either be done by means of the Comsol user interface or by starting the solution procedure directly from Matlab using the Livelink module and extending MCPlas accordingly. The Comsol user interface is used here to perform the analysis (cf. Fig. 1).

### III. RESULTS AND DISCUSSION

The application of MCPlas results in a system of fluid equations coupled with Poisson's equation as typically used for the numerical analysis of non-thermal plasmas for which a hydrodynamic description is valid. The following subsections first present and discuss the important features of the automated model implementation provided by MCPlas. Second, they illustrate the robustness and applicability of the model provided by MCPlas for the analysis of DBDs using two test cases.

#### A. Automation of model implementation

1) *Governing equations:* The automatically generated Comsol model comprises balance equations for the particle number densities  $n_p$  of the plasma species  $p$  (electrons, various ions and neutral particles in their ground and excited states) specified by the input files

$$\frac{\partial n_p}{\partial t} + \nabla \cdot \mathbf{\Gamma}_p = S_p, \quad (1)$$

the electron energy balance equation for the energy density of electrons  $w_e$

$$\frac{\partial w_e}{\partial t} + \nabla \cdot \mathbf{Q}_e = -e_0 \mathbf{E} \cdot \mathbf{\Gamma}_e + \tilde{S}_e, \quad (2)$$

and Poisson's equation for the electric potential  $\phi$

$$-\varepsilon_0 \varepsilon_r \nabla^2 \phi = \sum_p q_p n_p. \quad (3)$$

Here,  $\mathbf{\Gamma}_p$  and  $\mathbf{Q}_e$  are the particle fluxes and the electron energy flux,  $S_p$  and  $\tilde{S}_e$  are source terms describing the gain and loss of particles and electron energy due to reaction kinetic processes,  $e_0$  denotes the elementary charge,  $\mathbf{E} = -\nabla\phi$  is the electric field,  $\varepsilon_0$  and  $\varepsilon_r$  represent the vacuum permittivity and relative permittivity of the medium, respectively, and  $q_p$  is the charge of species  $p$ . For the fluxes of particles and the electron energy flux, the drift-diffusion approximations

$$\begin{aligned} \mathbf{\Gamma}_p &= \text{sgn}(q_p) b_p \mathbf{E} n_p - \nabla(D_p n_p), \\ \mathbf{Q}_e &= -\tilde{b}_e \mathbf{E} w_e - \nabla(\tilde{D}_e w_e) \end{aligned} \quad (4)$$

are used, where  $b_p$  and  $D_p$  are the mobility and diffusion coefficients for species  $p$ , and  $\tilde{b}_e$  and  $\tilde{D}_e$  are the mobility and diffusion coefficient for energy transport of electrons, respectively.

Note that the basic set of differential equations can be changed by modifying the MCPlas programme code, e.g. to take into account an equation and additional terms for the gas flow velocity or to use different kinds of approximations for

the fluxes. It should be also mentioned that MCPlas provides an option to solve these balance equations in logarithmic representation, where the equations are solved for the logarithm of the particle number density and the electron energy density. This prevents large scale variations and possible negative values in the solution.

2) *Boundary and initial conditions:* For Poisson's equation, Dirichlet boundary conditions are set, i.e. the potential is set to  $\phi = 0$  at the grounded electrode, and  $\phi = U_a$  at the powered electrode. Here,  $U_a$  denotes the applied voltage, which can be constant or given as a time-dependent function describing the temporal evolution of the voltage signal.

For modelling of DBDs, the additional interface condition  $-\varepsilon_0 \varepsilon_r \mathbf{E} \cdot \boldsymbol{\nu} = \sigma$  is used at the plasma-dielectric interface to account for the change of the electric field due to accumulated surface charges. In this case, the balance equation

$$\frac{\partial \sigma}{\partial t} = \sum_p q_p \Gamma_p \cdot \boldsymbol{\nu} \quad (6)$$

for the surface charge density  $\sigma$  accumulated at the dielectric boundaries facing to the plasma volume is added to the model, where  $\boldsymbol{\nu}$  is the outward normal vector to the respective boundary surface [13].

For the particle balance equations, boundary conditions according to Hagelaar *et al.* [23] are applied

1) for the balance equation (1) of heavy particles

$$\boldsymbol{\nu} \cdot \boldsymbol{\Gamma}_p = \frac{1 - r_p}{1 + r_p} \left( |b_p \mathbf{E} n_p| + \frac{1}{2} v_{th,p} n_p \right); \quad (7)$$

2) for the balance equation (1) of electrons

$$\begin{aligned} \boldsymbol{\nu} \cdot \boldsymbol{\Gamma}_e &= \frac{1 - r_e}{1 + r_e} \left( |b_e \mathbf{E} n_e| + \frac{1}{2} v_{th,e} n_e \right) \\ &\quad - \frac{2}{1 + r_e} \gamma \sum_i \max(\boldsymbol{\Gamma}_i \cdot \boldsymbol{\nu}, 0); \end{aligned} \quad (8)$$

3) for the electron energy balance equation (2)

$$\begin{aligned} \boldsymbol{\nu} \cdot \mathbf{Q}_e &= \frac{1 - r_e}{1 + r_e} \left( \tilde{b}_e \mathbf{E} w_e + \frac{1}{2} \tilde{v}_{th,e} w_e \right) \\ &\quad - \frac{2}{1 + r_e} u_e^\gamma \gamma \sum_i \max(\boldsymbol{\Gamma}_i \cdot \boldsymbol{\nu}, 0). \end{aligned} \quad (9)$$

Here,  $v_{th,p}$  is the thermal velocity of the respective species,  $\tilde{v}_{th,e} = 2k_B T_e v_{th,e}$  with the Boltzmann constant  $k_B$  and electron temperature  $T_e = 2w_e / (3k_B n_e)$ ,  $r_p$  are the reflection coefficients of species  $p$ ,  $\gamma$  is the secondary electron emission coefficient, and  $u_e^\gamma$  denotes the mean energy of secondary electrons. It should be noted that other sets of boundary conditions can be implemented as well by modifying the corresponding module of the MCPlas toolbox.

As initial values, quasi-neutral conditions with uniform number densities for all particle species are used. Similarly, the initial electron energy density is assumed to be uniform.

3) *Source terms:* The source terms  $S_p$  and  $\tilde{S}_e$  are defined as

$$S_p = \sum_{j=1}^{N_r} (G_{pj} - L_{pj}) R_j, \quad (10)$$

$$\tilde{S}_e = \sum_{j=1}^{N_r} \Delta \varepsilon_j R_j, \quad (11)$$

where  $R_j$  is the reaction rate

$$R_j = k_j \prod_{i=1}^{N_s} n_i^{\beta_{ij}}. \quad (12)$$

Here, the parameter  $\beta_{ij}$  is the partial reaction order of species  $i$  in reaction  $j$ ,  $k_j$  is the reaction rate coefficient for reaction  $j$ ,  $\Delta \varepsilon_j$  represents the electron energy gained or lost in reaction  $j$ , and  $N_r$  and  $N_s$  are the number of reactions and species, respectively. The gain ( $G_{pj}$ ) and loss ( $L_{pj}$ ) matrix elements in equation (10) are defined by the stoichiometric coefficients for the given species and reactions. MCPlas automatically generates these matrices from the species list and reaction scheme as described in section II. With this, the transition between models of different complexity in terms of the number of considered species and reactions is simplified. This provides the option, e.g. to easily perform studies on the influence of changes in the considered reaction kinetic model.

4) *Reaction rate and transport coefficients:* The plasma model implemented by MCPlas involves the rate coefficients for the collision and radiation processes as well as the transport coefficients for all considered species as variable definitions, look-up tables or analytical functions. The particular form of the coefficients depends on the given input files specifying the constant value or functional form. Various plasma quantities or geometrical parameters can be used as parameters for the function definitions, such as electric field, mean electron energy, gas temperature or characteristic lengths of the system.

A great benefit of this flexibility is that the set of coefficients can be exchanged without additional implementation effort. Thus it is easy, e.g. to switch between the local mean energy approximation and the local field approximation for definition of the coefficients of the electron component [24]–[26].

5) *Geometry and mesh:* Besides implementation of the various equations with their source terms and coefficients, the application of MCPlas results in a proper definition of the coordinates and boundary system for the given geometry. MCPlas supports spatially one-dimensional and two-dimensional models in Cartesian and cylindrical coordinates, so far. The geometry is either created by the Livelink module based on the setup parameters or read from a geometry file prepared in advance. Furthermore, MCPlas associates the boundary conditions (7)–(9) with the respective boundaries and interfaces of the computational domain. This is achieved by the definition of domain and boundary selections.

Once the geometry is set up, the prescribed element sizes for the given domain selections result in an automated generation of the mesh, which might be refined in selected regions. The possibility of exchanging the geometry for a given plasma

model via MCPlas and the automated mesh generation provided by Comsol allows to investigate various setups without additional implementation effort.

### B. Test cases

Two DBDs in argon at different conditions are used as test cases. Both test cases use the same number of species and the same reaction kinetic model for the spatiotemporal description of the discharge behaviour in diffuse DBD (first test case) and in a single-filament configuration (second test case), respectively. The model takes into account electrons plus 22 heavy particle species participating in 409 reaction kinetic processes. A list of the considered argon species with the corresponding energy levels is given in Table I.

TABLE I  
LIST OF HEAVY PARTICLE SPECIES CONSIDERED IN THE TWO TEST CASES.

Species	Energy level [eV]
Ar[1p <sub>0</sub> ]	0
Ar[1s <sub>5</sub> ]	11.55
Ar[1s <sub>4</sub> ]	11.62
Ar[1s <sub>3</sub> ]	11.72
Ar[1s <sub>2</sub> ]	11.82
Ar[2p <sub>10</sub> ]	12.91
Ar[2p <sub>9</sub> ]	13.08
Ar[2p <sub>8</sub> ]	13.09
Ar[2p <sub>7</sub> ]	13.15
Ar[2p <sub>6</sub> ]	13.17
Ar[2p <sub>5</sub> ]	13.27
Ar[2p <sub>4</sub> ]	13.28
Ar[2p <sub>3</sub> ]	13.30
Ar[2p <sub>2</sub> ]	13.33
Ar[2p <sub>1</sub> ]	13.40
Ar <sup>*</sup> [hl]	13.84
Ar <sup>+</sup>	15.76
Ar <sub>2</sub> <sup>*</sup> [ <sup>3</sup> Σ <sub>u</sub> <sup>+</sup> , v = 0]	9.76
Ar <sub>2</sub> <sup>*</sup> [ <sup>1</sup> Σ <sub>u</sub> <sup>+</sup> , v = 0]	9.84
Ar <sub>2</sub> <sup>*</sup> [ <sup>3</sup> Σ <sub>u</sub> <sup>+</sup> , v ≫ 0]	11.37
Ar <sub>2</sub> <sup>*</sup> [ <sup>1</sup> Σ <sub>u</sub> <sup>+</sup> , v ≫ 0]	11.45
Ar <sub>2</sub> <sup>+</sup>	14.50

The local-mean-energy approximation [26] is applied for the electron component, i.e. the rate coefficients for particle and energy transfer processes due to elastic collisions and various inelastic (e.g. exciting, de-exciting, ionizing) collisions of electrons as well as the electron transport coefficients are determined in advance by solving the stationary, spatially homogeneous electron Boltzmann equation in multi-term approximation [27]. These data are provided in the form of look-up tables as a function of the mean electron energy and used as input files for MCPlas. Further details about the reaction kinetics and transport properties are given in [28]. The reflection coefficients of electrons, ions and excited argon atoms as well as the secondary electron emission coefficient and corresponding energy of secondary electrons are taken as in [13].

Once the input files are prepared, execution of MCPlas takes only few tens of seconds to build up the Comsol models for the two test cases described in the following subsections.

#### 1) Modelling of a diffuse DBD in argon at 500 mbar:

The first test case for the application of MCPlas is the time-dependent and spatially one-dimensional (1D) modelling of an argon DBD at 500 mbar in plane-parallel configuration, where both electrodes are covered by glass dielectrics ( $\epsilon_r = 4.2$ ,  $\gamma = 0.02$ ) as illustrated in Fig. 2. The model setup is the same as used in Stankov *et al.* [28]. The gap between the 1 mm

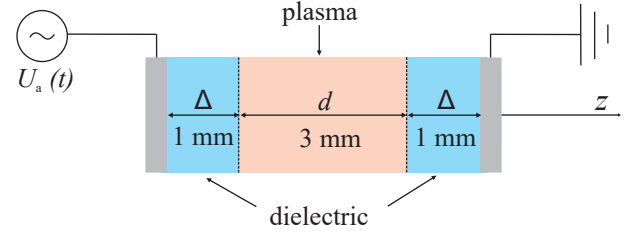


Fig. 2. Schematic description of the spatially one-dimensional DBD geometry used in test case 1.

thick dielectric layers is  $d = 3$  mm. The spatial variation of the plasma in the gap takes place along the  $z$ -axis between  $z = 1$  mm (left side) and  $z = 4$  mm (right side). The diffuse gas discharge is uniform perpendicular to this axis and has a cross-sectional area of  $A = 7.26$  cm<sup>2</sup>. The gas temperature is assumed to be constant at  $T_g = 300$  K. The sinusoidal voltage  $U_a(t) = U_0 \sin(2\pi ft)$  is applied at the left electrode, while the right electrode is grounded. The applied voltage has an amplitude of  $U_0 = 2$  kV and a frequency of  $f = 13.7$  kHz. Hence the period duration is equal to  $T = 73$  μs. The computational domain is divided into the plasma region with 1500 mesh elements and the dielectric part with 50 elements. Initial values of number densities for all species are assumed to be uniform with a number density of  $10^{12}$  m<sup>-3</sup> for heavy particles and  $2 \times 10^{12}$  m<sup>-3</sup> for the electrons.

Once the Comsol model is set up by using MCPlas, various discretisation methods and parameters can be set to optimise the solution procedure. Here, the finite element method with linear Lagrange elements is used for the balance equations of particle number densities and the electron energy balance equation, while quadratic Lagrange elements are applied for the Poisson equation. Discontinuous Lagrange elements of the first order are employed for the balance equation of surface charges. For the temporal discretisation, the backward differentiation formula with adaptive order varying between 1 and 5 is applied. The complete set of equations is solved in a fully coupled manner and the time-dependent solver utilizes the constant Newton method with damping factor equal to 1. The direct solver PARDISO is used for solving the system of linear equations. For present calculations the prescribed absolute and relative tolerances are set to  $10^{-4}$ . It was found that these values are adequate to achieve the required accuracy without hindering an efficient solution of the highly non-linear problem. Note that the balance equations are solved in logarithmic form to achieve better stability and no additional scaling is used for the solution variables. The calculation was carried out on a computer with two Intel<sup>®</sup> Xenon<sup>®</sup> E5-2667

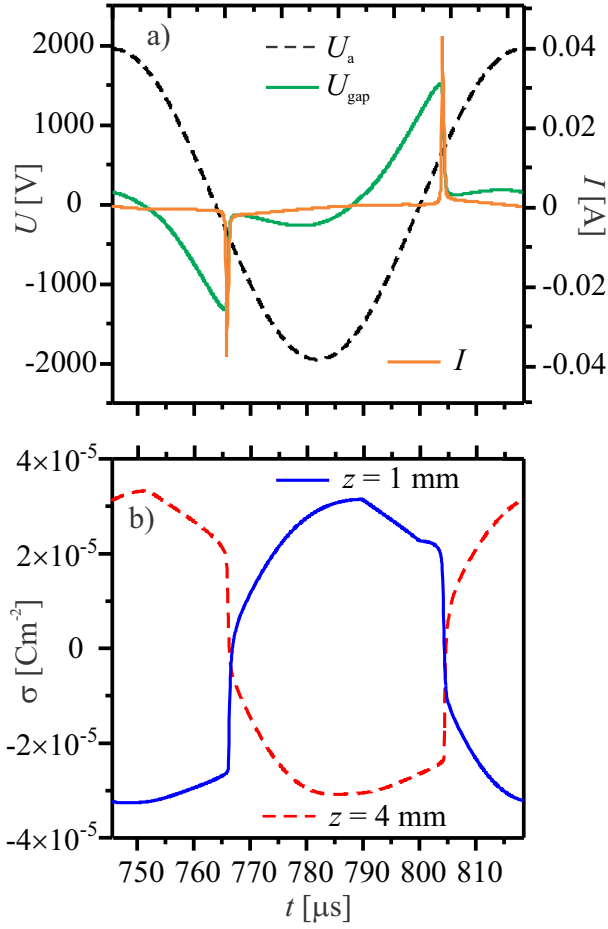


Fig. 3. Temporal evolution of a) discharge current  $I$  and gap voltage  $U_{\text{gap}}$  together with the voltage applied at the powered electrode  $U_a$  and b) surface charge density  $\sigma$  on the dielectrics at  $z = 1$  mm and  $z = 4$  mm obtained by model calculations for  $p = 500$  mbar,  $U_0 = 2$  kV and  $f = 13.7$  kHz (test case 1).

v2 @ 3.30GHz CPUs and with 125 Gb of RAM available in total. The calculations were carried out on 4 cores and lasted around 1.5 hours per period.

The calculated discharge current  $I$  and gap voltage  $U_{\text{gap}}$  for the periodic state of the discharge are shown in Fig. 3a). Characteristic current peaks corresponding to the breakdown events can be noticed from the results. The temporal evolution of the gap voltage is in correlation with the calculated current showing the fast decrease at the moment of breakdown, which is caused by the charging of the dielectrics. This is illustrated by the representation of the surface charge density  $\sigma$  in Fig. 3b).

The discharge current is mainly determined by the motion of electrons and the maximum number density of electrons is reached at the moment of the highest current. This becomes obvious from the spatiotemporal evolution of the electron number density  $n_e$  presented in Fig. 4. It can be seen that the highest number density of electrons appears at the instant of breakdown in front of the momentary cathode.

Fig. 5 shows the spatial distribution of the number densities of molecular ( $\text{Ar}_2^+$ ) and atomic ( $\text{Ar}^+$ ) ions and electrons as well as the magnitude of the electric field at the moment of

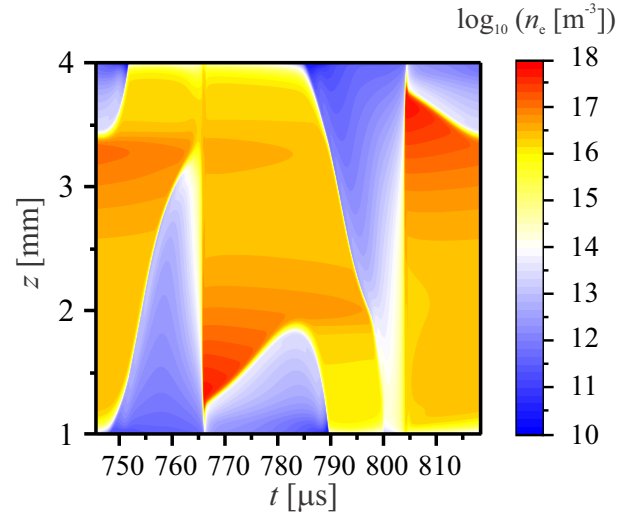


Fig. 4. Spatiotemporal behaviour of the electron number density during one period for the conditions of Figure 3 (test case 1).

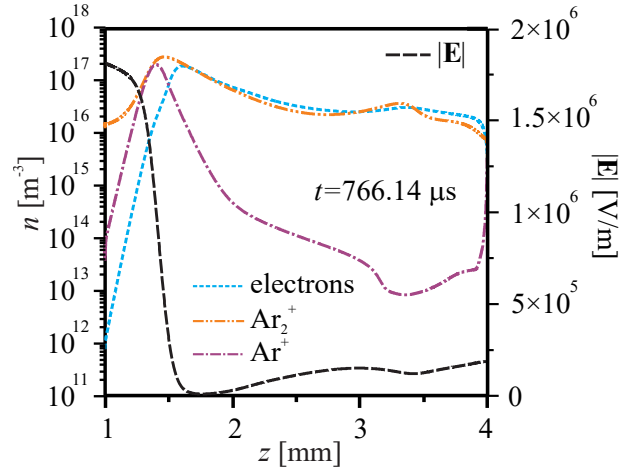


Fig. 5. Spatial variation of the number densities of electrons,  $\text{Ar}^+$  and  $\text{Ar}_2^+$  as well as of the magnitude of the electric field at the moment of maximum current ( $t = 766.14 \mu\text{s}$ ) for the conditions of Figure 3 (test case 1).

maximum current in the negative half-period ( $t = 766.14 \mu\text{s}$ ). Due to strong conversion of  $\text{Ar}^+$  in three-body collisions with two argon atoms, molecular argon ions are the dominant ionic species at these conditions. Electron and ions almost balance each other out in large parts of the discharge region. In front of the momentary cathode ( $z = 1$  mm), the number densities of ions are higher than the number density of electrons. This leads to the formation of the cathode sheath with high electric field. The presented results for this test case are in accordance with results obtained by model calculations for a similar type of DBD, reported e.g. in [29].

2) *Modelling of a single-filament DBD in argon at atmospheric pressure:* The second test case deals with time-dependent and spatially two-dimensional (2D) modelling of a single-filament atmospheric-pressure DBD in argon. The asymmetric configuration is shown in Fig. 6. It consists of two hemispherical electrodes with radius  $R = 2$  mm and gap width  $d = 1.5$  mm, in accordance with the setup described in [30].

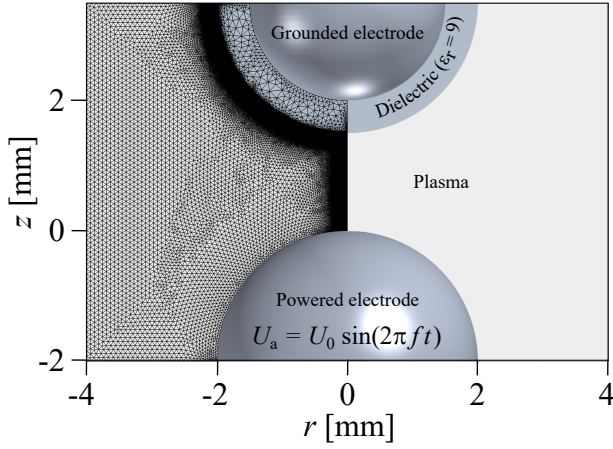


Fig. 6. Electrode setup of the asymmetric DBD configuration, along with the illustration of the mesh used in test case 2.

Here, the curved electrodes are used to fix one filament at the position with shortest electrode distance. The grounded electrode is covered with a dielectric (alumina,  $\epsilon_r = 9$ ,  $\gamma = 0.02$ , thickness  $\Delta = 0.5$  mm), and the metallic electrode (stainless steel,  $\gamma = 0.07$ ) is powered by the sinusoidal voltage  $U_a(t) = U_0 \sin(2\pi ft)$ . The voltage amplitude is set to be  $U_0 = 3$  kV and the frequency is  $f = 60$  kHz.

The focus of the analysis is on the streamer-induced first breakdown event during the first half-period. In this case, there are no volume and surface charges present in the gap or at the dielectric when the voltage is applied. In contrast to test case 1, a 2D model is required to fully describe the transient discharge dynamics and the formation of the constricted discharge channel occurring in the considered geometry at atmospheric pressure [30]. Due to the high computational costs, the discharge is considered to be axisymmetric for simplification and the model equations are solved in cylindrical coordinates.

The solution procedure is similar to that described for test case 1. In order to reduce the number of degrees of freedom and consequently the computation time, linear Lagrange elements are used here for all equations. Additionally, manual re-meshing of the domain is done to further reduce memory usage and the calculation time. For the pre-phase, covering the process of volume charge accumulation, a mesh consisting of approximately 60 000 elements is used, whereas for the streamer phase about 500 000 elements are required to resolve the steep gradients occurring at the streamer head. As shown in Fig. 6 the mesh is refined near the symmetry axis and the dielectric surface with maximum element size of  $4 \mu\text{m}$  near the axis and a mesh size varying between  $0.1$  and  $1.3 \mu\text{m}$  near the plasma-dielectric interface boundary. In the other parts of the domain, the mesh is much coarser. The calculations were carried out on a computer with two Intel® Xeon E5-2690 CPUs, having in total 128 Gb of RAM. The calculations were carried out using 4 cores and in total lasted approximately one week for the presented time-range.

Finally, it should be noted that the electric current is calculated as an integral of the sum of conduction and displacement

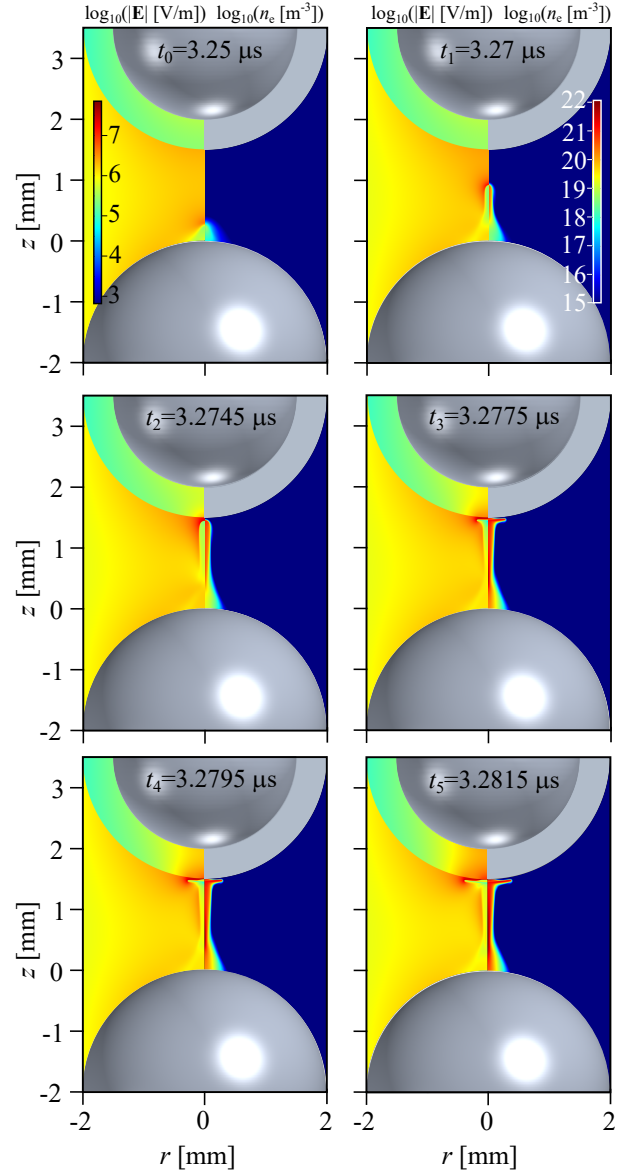


Fig. 7. Spatiotemporal development of the cathode-directed streamer illustrated by the evolution of the electric field magnitude (left-hand-side panel) and electron number density (right-hand-side panel) in characteristic times ( $t_0$ – $t_5$ ), noting that the logarithm of these quantities is used for better illustration, and that scales span over the whole time range (test case 2).

current density over the electrode surface using the relation

$$I = \int_S \left[ \sum_p q_p \Gamma_p \cdot \boldsymbol{\nu} + \epsilon_0 \frac{d\mathbf{E}}{dt} \cdot \boldsymbol{\nu} \right] dS, \quad (13)$$

where  $S$  is the surface area of the bare electrode directly exposed to plasma.

In order to illustrate the streamer development, the electron number density and magnitude of the electric field at six characteristic times  $t_0$  to  $t_5$  are presented in Fig. 7. With increase of the applied voltage, Townsend's phase (pre-phase) commences, during which the accumulation of space charges near the instantaneous anode occurs. When the critical density of charged particles is reached (approx.  $10^{18} \text{ m}^{-3}$ ), the streamer phase is initiated (cf.  $t_0$  in Fig. 7). The positive

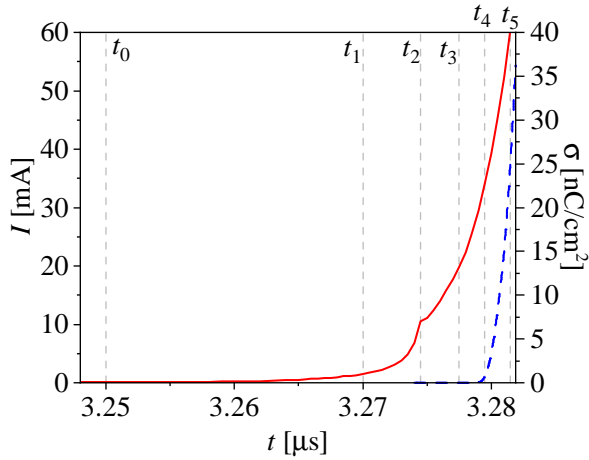


Fig. 8. Temporal evolution of the electric current  $I$  (solid red line) and surface charge density  $\sigma$  at the centre of the electrode, i.e. at  $r = 0$  (dashed blue line) with markers of the characteristic times  $t_0$  to  $t_5$  corresponding to the spatial profiles presented in Fig. 7.

streamer propagation starts in the anode region at  $z \approx 0.3$  mm. As the streamer propagates towards the cathode (cf.  $t_1$  in Fig. 7) a steep increase of the electric current  $I$  can be observed, as displayed in Fig. 8. At this point, there are no surface charges accumulated on the dielectric (cf.  $t_1$ – $t_2$  in Fig. 8). Simultaneously, the diameter and magnitude of the electric field increase, reaching its maximum in the vicinity of the cathode (cf.  $t_2$  in Fig. 7). Based on the full-width at half-maximum of the radial profile of the electron number density, the streamer diameter is determined to be  $72 \mu\text{m}$ . Note that the method described in Nijdam *et al.* [31] was used for determination of the streamer radius.

The moment when the streamer reaches the cathode (cf.  $t_2$  in Fig. 7) manifests as a local maximum (“hump”) in the electric current (cf. Fig. 8), as also observed in [32]. Upon reaching the cathode, the streamer starts propagating along the dielectric surface (cf.  $t_3$  to  $t_5$  in Fig. 7). At the same time the surface charge density starts to increase around  $t_4$  (cf. Fig. 8).

Fig. 9 shows the spatial variation of the magnitude of the electric field on the symmetry axis for different times. A gradual increase of the maximum of  $|\mathbf{E}|$  from about 5 to 47 MV/m is found as the streamer propagates towards the dielectric surface on the cathode side.

Fig. 10 illustrates the velocity of the streamer as obtained from the movement of the electric field maximum during streamer propagation. It can be observed that the streamer velocity increases as the streamer propagates in the gap. This is in agreement with results of measurements obtained for single-filament DBDs in argon and nitrogen-oxygen gas mixtures for similar geometries [33], [34]. A maximum streamer velocity of  $0.2 \text{ mm/ns}$  is reached in the vicinity of the cathode (cf.  $t_2$  in Fig. 7), which is in accordance with experimental results for argon DBDs [33] and about one order of magnitude lower than the streamer velocity observed in [34] for a nitrogen-oxygen DBD.

In comparison to the volume propagation, the velocity of the subsequent streamer propagation along the dielectric

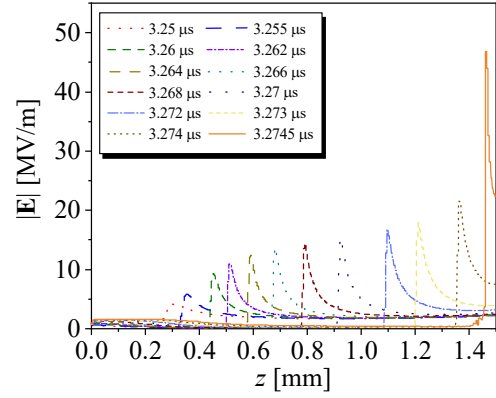


Fig. 9. Spatial distribution of the magnitude of the electric field on the symmetry axis for different times  $t$  during the volume propagation of the streamer up to  $t \approx t_2$ .

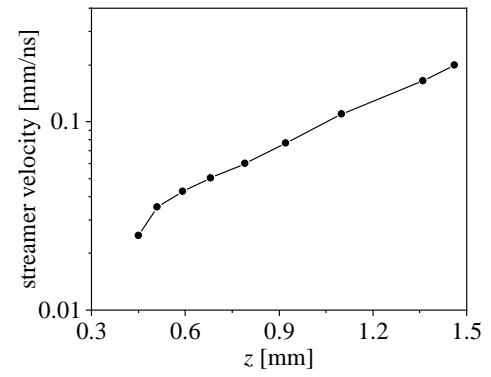


Fig. 10. Spatial (i.e. temporal) development of the streamer velocity in the gap during propagation of the streamer head from the anode side (left) towards the cathode (right). The maximum velocity is observed at  $t \approx t_2$  in the vicinity of the dielectric boundary on the cathode side at  $z = 1.5$  mm.

surface is smaller by one order of magnitude. The surface streamer propagation continues until a sufficient amount of surface charges is accumulated on the dielectric, leading to the reduction of the electric field and charge carrier production in this region. It is expected that the surface propagation does not occur rotationally uniform but in form of constricted filaments as observed in nitrogen-oxygen DBDs [35]. Thus, the validity of the present axisymmetric model is limited as soon as the streamer starts to spread along the dielectric surface. Further experimental and computational analyses of the surface streamer propagation for the present DBD setup will be part of future investigations.

#### IV. SUMMARY

Fluid modelling is a powerful tool for the analysis of the physical and chemical processes of gas discharge plasmas and their applications. However, the management of the equations and source term generation as well as the definition of all required transport and rate coefficients can be a tedious and error-prone process, particularly when lots of species need to be taken into account.

It is shown how the MCPlas toolbox helps to tremendously speed up the process of model implementation by means

of automation. This is achieved by combining functionalities provided by Comsol and Matlab. Besides the time-saving aspect, automation virtually eliminates the possibility for errors, which are characteristic for manual implementations of complex reaction kinetic models. Furthermore, it is discussed how MCPlas supports studies on the influence of different reaction kinetic models and how it facilitates the seamless transition between different model geometries in spatially 1D and 2D configurations.

The practical applicability of the MCPlas toolbox as well as the Comsol model provided by MCPlas is illustrated by two case studies dealing with the analysis of a diffuse and a filamentary DBD in argon. These examples also demonstrated the advantages of automated code generation by using the same plasma model to study a diffuse discharge in symmetric 1D geometry and a filamentary DBD in asymmetric 2D geometry. Implementing the two different models on the basis of the same input files (except for the geometry and discharge parameters) takes only few tens of seconds.

The presented results confirm that even complex processes like the interaction of streamers with dielectric surfaces can be investigated using the models obtained by means of the MCPlas toolbox. An extension of MCPlas to provide the option for spatially three-dimensional geometries is technically possible without further ado. However, the computing time will then be a strongly limiting factor on present computing architectures.

#### ACKNOWLEDGMENT

This work is funded by the Deutsche Forschungsgemeinschaft (DFG, German Research Foundation) - project numbers 368502453 and 407462159.

#### REFERENCES

- [1] M. Kogoma and S. Okazaki, "Raising of ozone formation efficiency in a homogeneous glow discharge plasma at atmospheric pressure," *J. Phys. D: Appl. Phys.*, vol. 27, no. 9, pp. 1985–1987, 1994.
- [2] A. Fridman, A. Chirokov, and A. Gutsol, "Non-thermal atmospheric pressure discharges," *J. Phys. D: Appl. Phys.*, vol. 38, no. 2, pp. R1–R24, 2005.
- [3] U. Kogelschatz, B. Eliasson, and W. Egli, "Dielectric-barrier discharges. Principle and applications," *J. Phys. IV France*, vol. 07, no. C4, pp. 47–66, 1997.
- [4] U. Kogelschatz, "Dielectric-barrier discharges: Their history, discharge physics, and industrial applications," *Plasma Chem. Plasma Process.*, vol. 23, no. 1, pp. 1–46, 2003.
- [5] R. Brandenburg, "Dielectric barrier discharges: progress on plasma sources and on the understanding of regimes and single filaments," *Plasma Sources Sci. Technol.*, vol. 26, no. 5, p. 053001, 2017.
- [6] U. Kogelschatz, "Filamentary, patterned, and diffuse barrier discharges," *IEEE Trans. Plasma Sci.*, vol. 30, no. 4, pp. 1400–1408, 2002.
- [7] D. Braun, V. Gibalov, and G. Pietsch, "Two-dimensional modelling of the dielectric barrier discharge in air," *Plasma Sources Sci. Technol.*, vol. 1, no. 3, pp. 166–174, 1992.
- [8] G. Steinle, D. Neundorff, W. Hiller, and M. Pietralla, "Two-dimensional simulation of filaments in barrier discharges," *J. Phys. D: Appl. Phys.*, vol. 32, no. 12, pp. 1350–1356, 1999.
- [9] V. I. Gibalov and G. J. Pietsch, "The development of dielectric barrier discharges in gas gaps and on surfaces," *J. Phys. D: Appl. Phys.*, vol. 33, no. 20, pp. 2618–2636, 2000.
- [10] L. Papageorghiou, E. Panousis, J. F. Loiseau, N. Spyrou, and B. Held, "Two-dimensional modelling of a nitrogen dielectric barrier discharge (DBD) at atmospheric pressure: filament dynamics with the dielectric barrier on the cathode," *J. Phys. D: Appl. Phys.*, vol. 42, no. 10, p. 105201, 2009.
- [11] V. I. Gibalov and G. J. Pietsch, "Dynamics of dielectric barrier discharges in different arrangements," *Plasma Sources Sci. Technol.*, vol. 21, no. 2, p. 024010, 2012.
- [12] J.-P. Boeuf, L. L. Yang, and L. C. Pitchford, "Dynamics of a guided streamer ('plasma bullet') in a helium jet in air at atmospheric pressure," *J. Phys. D: Appl. Phys.*, vol. 46, p. 015201, 2013.
- [13] M. M. Becker, T. Hoder, R. Brandenburg, and D. Loffhagen, "Analysis of microdischarges in asymmetric dielectric barrier discharges in argon," *J. Phys. D: Appl. Phys.*, vol. 46, no. 35, p. 355203, 2013.
- [14] "COMSOL Multiphysics® v. 5.5. COMSOL AB, Stockholm, Sweden." [www.comsol.com](http://www.comsol.com).
- [15] "Matlab, version R2018b," Natick, Massachusetts.
- [16] M. Šimek and Z. Bonaventura, "Non-equilibrium kinetics of the ground and excited states in N<sub>2</sub>-O<sub>2</sub> under nanosecond discharge conditions: extended scheme and comparison with available experimental observations," *J. Phys. D: Appl. Phys.*, vol. 51, no. 50, p. 504004, 2018.
- [17] S. Ponduri, M. M. Becker, S. Welzel, M. C. M. van de Sanden, D. Loffhagen, and R. Engeln, "Fluid modelling of CO<sub>2</sub> dissociation in a dielectric barrier discharge," *J. Appl. Phys.*, vol. 119, no. 9, p. 093301, 2016.
- [18] C. De Bie, J. van Dijk, and A. Bogaerts, "The dominant pathways for the conversion of methane into oxygenates and syngas in an atmospheric pressure dielectric barrier discharge," *J. Phys. Chem. C*, vol. 119, no. 39, pp. 22 331–22 350, 2015.
- [19] C. Lazarou, T. Belmonte, A. S. Chiper, and G. E. Georghiou, "Numerical modelling of the effect of dry air traces in a helium parallel plate dielectric barrier discharge," *Plasma Sources Sci. Technol.*, vol. 25, no. 5, p. 055023, 2016.
- [20] D. Loffhagen, M. M. Becker, A. K. Czerny, and C.-P. Klages, "Modeling of atmospheric-pressure dielectric barrier discharges in argon with small admixtures of tetramethylsilane," *Plasma Chem. Plasma Process.*, vol. 41, no. 1, pp. 289–334, 2021.
- [21] A. P. Jovanović, M. N. Stankov, D. Loffhagen, and M. M. Becker, "Fluid modelling of dielectric barrier discharges for plasma technology," in *COMSOL Conference 2020 Europe*. COMSOL France SAS, October 14–15 2020.
- [22] B. Bagheri, J. Teunissen, U. Ebert, M. M. Becker, S. Chen, O. Ducasse, O. Eichwald, D. Loffhagen, A. Luque, D. Mihailova, J. M. Plewa, J. van Dijk, and M. Yousfi, "Comparison of six simulation codes for positive streamers in air," *Plasma Sources Sci. Technol.*, vol. 27, no. 9, p. 095002, 2018.
- [23] G. J. M. Hagelaar, F. J. de Hoog, and G. M. W. Kroesen, "Boundary conditions in fluid models of gas discharges," *Phys. Rev. E*, vol. 62, no. 1, pp. 1452–1454, 2000.
- [24] S.-K. Park and D. J. Economou, "Analysis of low pressure rf glow discharges using a continuum model," *J. Appl. Phys.*, vol. 68, no. 8, pp. 3904–3915, 1990.
- [25] G. J. M. Hagelaar and L. C. Pitchford, "Solving the Boltzmann equation to obtain electron transport coefficients and rate coefficients for fluid models," *Plasma Sources Sci. Technol.*, vol. 14, no. 4, pp. 722–733, 2005.
- [26] G. K. Grubert, M. M. Becker, and D. Loffhagen, "Why the local-mean-energy approximation should be used in hydrodynamic plasma descriptions instead of the local-field approximation," *Phys. Rev. E*, vol. 80, no. 3, p. 036405, 2009.
- [27] H. Leyh, D. Loffhagen, and R. Winkler, "A new multi-term solution technique for the electron Boltzmann equation of weakly ionized steady-state plasmas," *Comput. Phys. Commun.*, vol. 113, no. 1, pp. 33–48, 1998.
- [28] M. Stankov, M. M. Becker, R. Bansemer, K.-D. Weltmann, and D. Loffhagen, "Influence of surface parameters on dielectric-barrier discharges in argon at subatmospheric pressure," *Plasma Sources Sci. Technol.*, vol. 29, no. 12, p. 125009, 2020.
- [29] F. Massines, A. Rabehi, P. Decomps, R. B. Gadri, P. Ségur, and C. Mayoux, "Experimental and theoretical study of a glow discharge at atmospheric pressure controlled by dielectric barrier," *J. Appl. Phys.*, vol. 83, no. 6, pp. 2950–2957, 1998.
- [30] T. Hoder, D. Loffhagen, C. Wilke, H. Grosch, J. Schäfer, K.-D. Weltmann, and R. Brandenburg, "Striated microdischarges in an asymmetric barrier discharge in argon at atmospheric pressure," *Phys. Rev. E*, vol. 84, no. 4, p. 046404, 2011.
- [31] S. Nijdam, F. M. J. H. van de Wetering, R. Blanc, E. M. van Veldhuizen, and U. Ebert, "Probing photo-ionization: experiments on positive streamers in pure gases and mixtures," *J. Phys. D: Appl. Phys.*, vol. 43, no. 14, p. 145204, 2010.

- [32] I. Odrobina and M. Černak, "Numerical modeling of the streamer-cathode interaction in a short positive point-plane corona gap," *Czech. J. Phys.*, vol. 42, no. 3, pp. 303–315, 1992.
- [33] P. Kloc, H.-E. Wagner, D. Trunec, Z. Navrátil, and G. Fedoseev, "An investigation of dielectric barrier discharge in Ar and Ar/NH<sub>3</sub> mixture using cross-correlation spectroscopy," *J. Phys. D: Appl. Phys.*, vol. 43, no. 34, p. 345205, 2010.
- [34] H. Höft, M. M. Becker, and M. Kettlitz, "Correlation of axial and radial breakdown dynamics in dielectric barrier discharges," *Plasma Sources Sci. Technol.*, vol. 27, no. 3, p. 03LT01, 2018.
- [35] M. Kettlitz, H. Höft, T. Hoder, K.-D. Weltmann, and R. Brandenburg, "Comparison of sinusoidal and pulsed-operated dielectric barrier discharges in an O<sub>2</sub>/N<sub>2</sub> mixture at atmospheric pressure," *Plasma Sources Sci. Technol.*, vol. 22, no. 2, p. 025003, 2013.



**Markus M. Becker** was born in 1982 in Germany. He received the diploma degree in mathematics in 2008 and the Dr. rer. nat. degree in Computational Physics in 2012, both from the University of Greifswald. Since then, he is researcher and project manager at the Leibniz Institute for Plasma Science and Technology (INP) in Greifswald, Germany. His research interests include modelling and applications of dielectric barrier discharges, modelling approaches for non-thermal plasmas, and methods for sustainable data management in plasma science.



**Aleksandar P. Jovanović** was born in Knjaževac, Serbia in 1984. He graduated in physics in 2010 and received the Ph.D. degree in physics, both from the Faculty of Sciences and Mathematics, University of Niš, Serbia. From 2011 until 2018, he was employed as a researcher with the Department of Physics at the Faculty of Sciences and Mathematics in Niš. Since 2019, he is researcher with the Plasma Modelling Department, Leibniz Institute for Plasma Science and Technology (INP) in Greifswald, Germany. His research interest includes plasma modelling with

emphasis on electrical discharges (low pressure and DBD), physics of ionised gases, computational physics and statistics.



**Marjan N. Stankov** was born in 1985 in Serbia, where he completed elementary and grammar school. He graduated from the Department of Physics at the Faculty of Sciences and Mathematics in Niš in 2011 and finished his Ph.D. degree in 2015. He was working at the same university until the end of 2017 in the field of low-pressure DC glow discharge plasmas in argon and synthetic air. Since 2018, he is within Leibniz Institute for Plasma Science and Technology (INP) in Greifswald, focusing on hydrodynamic modelling of dielectric barrier

discharges for plasma-medical application and numerical modelling of microwave discharges suitable for deposition application.



**Detlef Loffhagen** was born in Neustadt am Rübenberge, Germany, on 22 September 1960. He received the Diploma and the Ph.D. degree in physics from University Hannover, Germany, in 1988 and 1992, respectively, and the Dr. rer. nat. habil. degree in theoretical plasma physics from University of Greifswald, Germany, in 2004. Between 1993 and 1994, he was with the Institute for Plasma Physics, University Hannover. Since May 1994, he has been with the Leibniz Institute for Plasma Science and Technology (INP), Greifswald, Germany, where he

became the head of the Department of Plasma Modelling in 2004. His research concerns gas discharge modelling, plasma chemistry, electron and ion kinetics, and plasma simulation.